Applied Mathematics, Modeling and Computer Simulation
C.-H. Chen et al. (Eds.)

doi:10.3233/ATDE221072

Investigation on the Effect of Anti-Braking System on Nose Landing Gear Shimmy

Jiaxian ZHANG[a], Jiliang TU[a,1], Hui LIU[a] and Shixue ZHANG[b]
[a]*School of Information Engineering, Nanchang Hangkong University, Jiangxi Nanchang 330063, China*
[b]*School of Finance and Trade, Zhengzhou Shengda University, Henan Zhengzhou 451191, China*

Abstract. The influence of anti-braking system on the shimmy region and oscillation characteristics of the nose landing gear is studied. The moment generated by the braking system is modeled as a function of the adhesion coefficient and the torsional oscillation speed, and it is incorporated into the landing gear oscillation non-linear dynamic model. The results of analysis show that the braking frequency is increased by 50%, the area of the lateral dominant shimmy region is increased by 6.9%, the area of the torsional dominant shimmy region is reduced by 18.8%, and the amplitude of the torsional oscillation is suppressed. The braking amplitude is increased by 22%, the area of lateral dominant shimmy region is decreased by 3.1%, and the area of torsional dominant shimmy region is increased by 15.5%.

Keywords. Anti-braking system, Nose landing gear, Shimmy, Nonlinear dynamics.

1. Introduction

Landing gear oscillation can impact its own structure and sometimes even cause serious safety accidents. The nose landing gear is more likely to oscillate during high-speed taxiing on the runway than the main landing gear[1]. Therefore, the study on the shimmy of the nose landing gear and the analysis of its influencing factors are very important to improve the safety of aircraft. Von Schlippe et al. [2] proposed a tire tension model to describe the interaction and vibration of the tire with the ground while it is rotating. Based on this theory, Thota et al. [3,4,5] coupled the torsional shimmy of the strut with the lateral shimmy, proposed a multi-degree-of-freedom coupled oscillation model of the nose landing gear, and used the bifurcation theory to analyze the effects of different types of shimmy on the dynamics of the landing gear. Based on the dynamic response and stability analysis of the landing gear oscillation damper, Arreaza et al. [6] proposed that the kinetic energy of the aircraft is transferred to the wheels and used as the main energy source to excite the oscillation. With the further research on shimmy analysis and modeling, the focus of current research has turned to the analysis of influencing factors of shimmy. Rahmani et al. [1,7,8] studied the effects of coulomb friction and clearance connecting rods on the shimmy of the nose landing gear. Thota et al. [9] studied the effect of changes in tire inflation pressure on the shimmy of the nose landing gear. Feng et al. studied the effects of wheel distance [10]

[1] Corresponding Author: Jiliang Tu , School of Information Engineering, Nanchang Hangkong University, Jiangxi Nanchang 330063, China; E-mail: 1271090531@qq.com

and torsional damping [11] on the shimmy area and topological structure of the nose landing gear. In order to study the influence of anti-braking system on landing gear shimmy, Yin et al. [12,13] established a physical model of coupling landing gear with braking wheel in LMS Virtual Lab Motion software, and used this model to study the influence of tire structure parameters and braking moment on landing gear shimmy stability. Chen et al. [14] set up a landing gear dynamic model in Simcenter 3D software to analyze the influence of symmetric and asymmetric brakes on the landing gear multi-degree of freedom coupled shimmy.

From the above literature, the impact of anti-braking system on landing gear shimmy is mainly focused on the impact of amplitude and shimmy speed. The research method mainly uses multi-body physical model combined with finite element analysis. Although this method can accurately identify the mechanical behaviour of each subsystem under different conditions, it can not meet many design updates in the optimization process when design optimization of the system is needed. In view of the above shortcoming, this paper establishes a mathematical model describing the braking and shimmy of landing gear, and models the moment generated by braking process as a function of the adhesion coefficient and the torsional shimmy speed. The study on the influence of anti-braking system on the shimmy region and oscillation characteristics of nose landing gear is carried out, which provides a reference for the design and structure optimization of aircraft nose landing gear.

2. Modeling of Landing Gear Shimmy and Braking Dynamics

2.1. Dynamic Modeling of Landing Gear Shimmy

Figure 1 shows the structural diagram of the nose landing gear. The nose landing gear is connected with the fuselage and has a certain front rake angle φ with the ground. When the aircraft taxis on the runway, the load imposed by the fuselage on the landing gear will cause the landing gear to produce torsional shimmy(shimmy angle ψ) around the strut axis and lateral shimmy(shimmy angle δ) around the fuselage axis. Under the joint influence of the two shimmy and the ground, the contact part between the tire and the ground will produce lateral deformation(deformation λ).

(a) front view (b) side view

Figure 1. View of nose landing gear structure

The dynamic equations of torsional and lateral shimmy can be expressed as equations (1) to (3).

$$I_z\ddot{\psi}+k_\psi\psi+c_\psi\dot{\psi}+M_{F1}+M_b+\frac{c_\lambda\dot{\psi}\cos(\varphi)}{V}-F_z\sin(\varphi)e_{eff}\sin(\psi\cos(\varphi))=0 \tag{1}$$

$$I_x\ddot{\delta}+k_\delta\delta+c_\delta\dot{\delta}+M_{\lambda\delta}-F_z e_{eff}\sin(\psi\cos(\varphi))=0 \tag{2}$$

$$\dot{\lambda}+\frac{V}{L}\lambda-V\sin(\psi\cos(\varphi))-L_g\dot{\delta}\cos(\delta)-(e_{eff}-h)\cos(\psi\cos(\varphi))\dot{\psi}\cos\varphi=0 \tag{3}$$

Equation (1) is the balance equation describing the degree of freedom of the landing gear torsional shimmy, where M_{F1} is the combined moment [15] of the torsional restoring moment and the tire lateral restoring moment, as shown in the following equation (4).

$$M_{F1}=M_{k\alpha}+e_{eff}F_{k\lambda} \tag{4}$$

Where $M_{k\alpha}$ is the torsional restoring moment and $F_{k\lambda}$ is the lateral restoring force of the tire, which can be calculated by equation (5) and equation (6) respectively.

$$M_{k\alpha}=\begin{cases} k_\alpha\dfrac{\alpha_m}{\pi}\sin\left(\alpha\dfrac{\pi}{\alpha_m}\right)F_{\{z\}} & if|\alpha|\leqslant\alpha_m \\ 0 & if|\alpha|\geqslant\alpha_m \end{cases} \tag{5}$$

$$F_{k\lambda}=k_\lambda\tan^{-1}(7\tan(\alpha))\cos(0.95\tan^{-1}(7\tan(\alpha)))F_z \tag{6}$$

where $\alpha=\tan^{-1}(\lambda/L)$ is the function of tire lateral deformation λ and relaxation length L.

Equation (2) is the balance equation describing the degree of freedom of the landing gear lateral shimmy, where $M_{\lambda\delta}$ is the lateral restoring moment of the tire deformation, as shown in equation (7).

$$M_{\lambda\delta}=L_g F_{k\lambda}\cos(\psi\cos\varphi)\cos\varphi \tag{7}$$

Equation (3) is the tire lateral deformation balance equation based on the tire tension theory, which can be regarded as the algebraic sum of the tire lateral deformation equation caused by torsional and lateral shimmy [3]. The meanings and values of parameters in this paper are shown in table 1 (some values in table 1 are from literature [1], literature [4] and the Internet).

Table. 1. Parameter meanings and values in the model

Parameter	Description	Value	Parameter	Description	Value
e_{eff}	effective caster length	0.2606 m	R	tire radius	0.362m
L_g	strut length	2.5 m	h	length of tire contact path	0.1m
k_ψ	torsional stiffness	$3.41*10^5$ Nm/rad	c_λ	damping coefficient of tire	$570Nm^2/rad$
c_ψ	torsional damping	110 Nm/rad	k_α	torsional restoring coefficient	1m/rad
I_z	torsional moment of inertia	$100kg*m^2$	k_λ	lateral restoring coefficient	0.01/rad
k_δ	lateral stiffness	$3.24*10^6$ Nm/rad	L	tire relaxation length	0.3m
c_δ	lateral damping	1 Nm/rad	α_m	slip angle limit	0.1745rad
I_x	lateral moment of inertia	$600kg*m^2$	r	strut radius	0.07m
φ	front rake angle	0.2571rad	M	aircraft mass	18000kg
σ	coefficient of dry friction	0.002	C	coefficient of air resistance	0.3415

2.2. Aircraft Brake Dynamics Modeling

The force analysis of the aircraft during braking is shown in figure 2. F_1 is the adhesion force between the ground and the tire during braking, and F_r is the air resistance during braking. They are represented by equations (8) and (9) respectively.

$$F_1 = \mu \cdot Mg \tag{8}$$

$$F_r = C \cdot V^2 \tag{9}$$

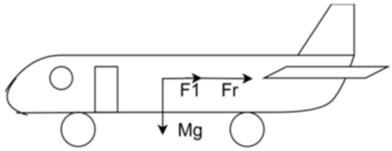

Figure 2. Force analysis of the aircraft during braking

When the anti-braking system is not started, there is no relative sliding between the tire and the ground, and the adhesion force F_1 is zero. On the contrary, the tire slips relative to the ground, thus creating a adhesion force [16]. In conclusion, based on the analysis of figure 2, the braking dynamic equation of the aircraft during taxiing is shown in the equations (10) and (11).

$$M\dot{V} = -\mu \cdot Mg - C \cdot V^2 \tag{10}$$

$$J\dot{\omega} = \frac{1}{3}\mu \cdot Mg \cdot R - M_{brake} \tag{11}$$

Equation (10) is the balance equation describing the horizontal speed V of the aircraft, where C is the air resistance coefficient and μ is the coefficient of the adhesion force of the tire and the ground, which can be calculated by the following equation (12) [17], where R is the tire radius.

$$\mu = 0.8\sin\left(1.5344\tan^{-1}\left(14.0326\frac{V - \omega \cdot R}{V}\right)\right) \tag{12}$$

Form (11) is a balance equation describing the angular speed of a tire, where M_{brake} is the moment applied to the tire by the anti-skid braking system. To ensure the operability of an aircraft during braking, this moment is usually a variable over time, and it is often simulated by a sine function in engineering [18]. The braking moment in this paper is expressed by the following equation (13).

$$M_{brake} = Amp\sin(2\pi ft) + Amp \tag{13}$$

Where Amp is the braking amplitude and f is the braking frequency.

2.3. Moment Generated by Actuating the Brake System

From M_b in equation (1) is the moment generated by the force acting on the landing gear strut when the braking system is activated, which hinders the torsional shimmy of the strut, as shown in the equation (14). Where r is the radius of the strut and F_t is the tangential component of the force on the strut. As shown in figure 3, the forces are shown in Formulas (15) and (16).

$$M_b = r \cdot F_t \tag{14}$$

$$\vec{F} = F_t\vec{e}_t + F_a\vec{e}_z \tag{15}$$

$$|F| = \mu F_z \sigma \tag{16}$$

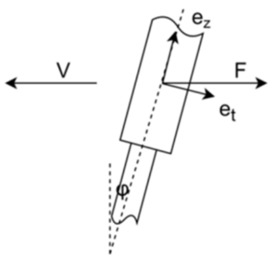

Figure 3. Decomposition of forces on landing gear strut

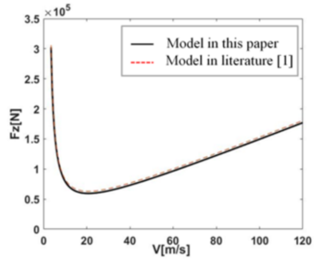

Figure 4. Model accuracy verification

Where F_z is the load applied on the strut, and σ is the dry friction coefficient between the inner and outer cylinders of the strut. According to the torsion speed of the strut, F_t can be obtained as shown in the following equation (17).

$$F_t = \mu F_z \sigma \cos(\varphi) \frac{\dot{\psi}}{|\dot{\psi}|} \tag{17}$$

3. Numerical Simulation Results and Analysis

3.1. Analysis of Landing Gear Shimmy without Braking

In order to verify the accuracy of the model described in this paper, based on the example in literature[1], the ode23tb solver in MATLAB is used to solve the solutions of the models described in this paper and those described in literature[1], and the results of stability analysis are shown in figure 4. It can be seen from figure 4 that the results of the two models are very close, and the trend of the curve is basically the same, which proves the accuracy of the model in this paper.

Based on the data in table 1 and the model described in Section 2.1, the maximum torsional and lateral shimmy amplitudes of the landing gear strut under different horizontal speeds V and loads F_z are calculated using MATLAB software, and the results are shown in figure 5. The dark blue area in figure 5 is the stable region without shimmy. According to figure 5 (b) and figure 5 (d), the region of torsional shimmy and lateral shimmy in the whole parameter region is shown in figure 6 (a).

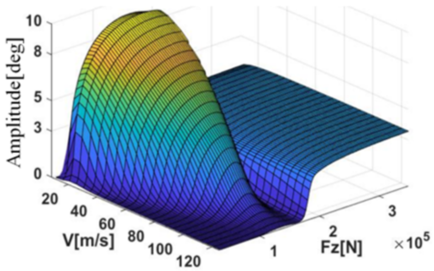

(a) rotational shimmy amplitude: main view

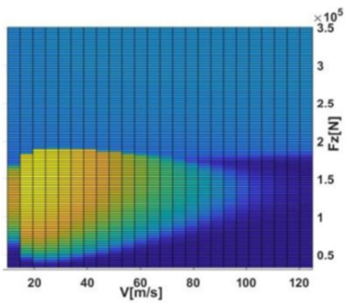

(b) rotational shimmy amplitude: top view

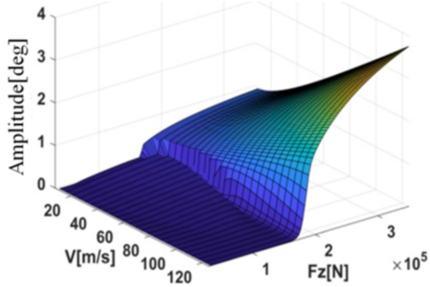

(c) lateral shimmy amplitude: main view

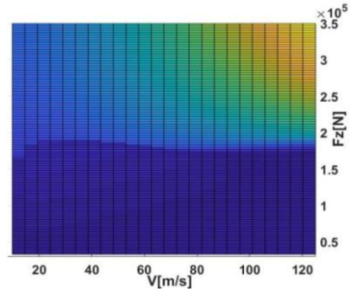

(d) lateral shimmy amplitude: top view

Figure 5. Shimmy amplitude and region

Figure 6(a) shows that the whole parameter space is divided into three parts. To verify the reliability of the results, the oscillation amplitude or the power spectrum of tire lateral deformation λ under corresponding parameters are calculated by taking points A, B and C in the figure. The results are shown in figure 6 (b-d), respectively. According to table 1, the natural frequencies of torsional and lateral shimmy are 9.3Hz and 11.7Hz, respectively. According to figure 6 (b-d), the oscillation of point A decays rapidly and no longer starts, so the point is in the stable region. Under the condition of point B, the oscillation frequency of λ is f = 9.34Hz, so the point is dominated by the torsional shimmy. Under the condition of point C, the oscillation frequency of λ is f = 11.73Hz, so the point is dominated by the lateral shimmy.

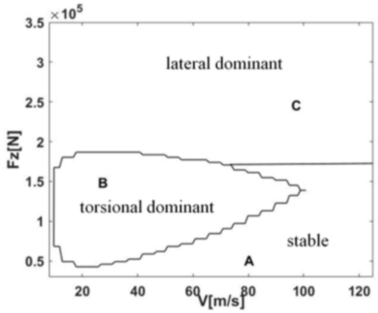

(a) shimmy region distribution

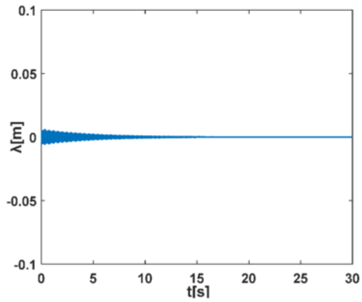

(b) point A(V=80m/s,F_z=50KN)

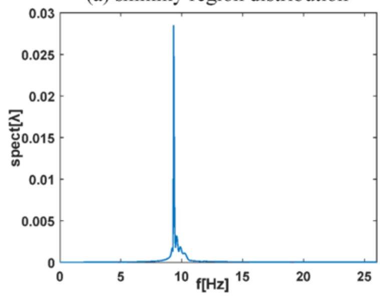

(c) point B(V=30m/s,F_z=150KN)

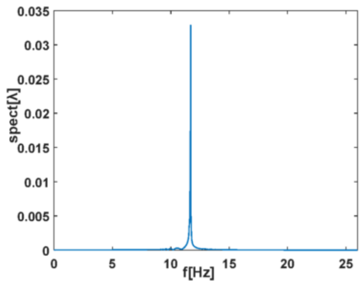

(d) point C(V=100m/s,F_z=250KN)

Figure 6. Region distribution and vibration characteristics

3.2. Analysis of landing Gear Shimmy under Braking Condition

Taking *amp*=9000, *f*=10hz as the basic braking parameters, calculate the variation relationship of the adhesion coefficient with the speed according to the model described in Section 2.2, and calculate the shimmy region distribution under the braking state in combination with the models described in Section 2.1 and Section 2.3. The results are shown in figure 7. Based on the above results, the relative changes of shimmy region area under braking are shown in table 2. From figure 7 and table 2, it can be seen that the braking system will reduce the area of the stable region and the torsional region, and increase the area of the lateral region. The impact on the torsional region is particularly significant, with an area change of 35.3%. The influence on the area of stable region is small, only 9%.

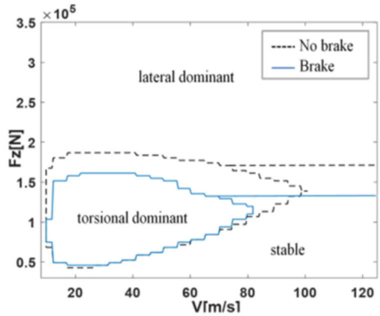

Figure 7. Comparison of shimmy region

Table 2. Comparison of relative area change of shimmy region

	stable area	torsional dominant area	lateral dominant area
No brake	551	607	1342
brake	501	393	1606
change	-9%	-35.3%	+16.4%

3.3. Influence of Braking Frequency and Braking Amplitude on Shimmy Region

Repeat the process in Section 3.2. Take *amp*=9000, *f*=5hz, 15Hz and *amp*=700011000, *f*=10hz respectively to explore the impact of different braking frequencies and braking amplitudes on the shimmy region. The results are shown in figure 8. It can be seen from figure 8 (a), taking 10Hz as the reference braking frequency, when the braking frequency increases to 15Hz, the torsional and stable domain area decrease, and the lateral domain area increases. When the braking frequency is reduced to 5Hz, the result is just the opposite. According to figure 8 (b), taking amp=9000 as the benchmark braking amplitude, when the braking amplitude increases to 11000, the torsional domain and stable domain area increase, and the lateral domain area decreases. When the braking amplitude decreases to 7000, the result is just the opposite. See table 3 for detailed comparison of shimmy region changes.

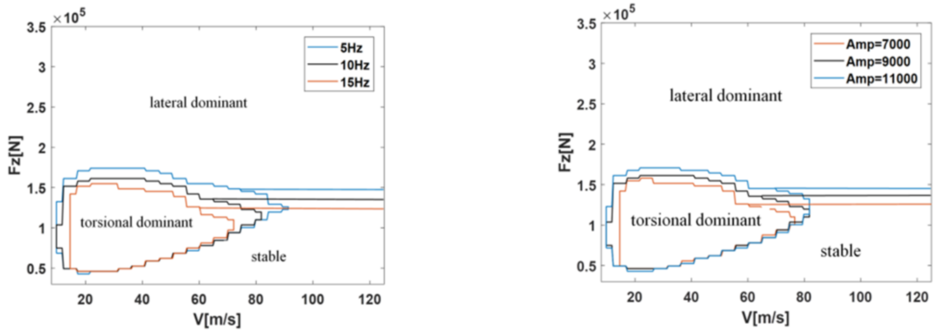

(a) Braking frequency (b) Braking amplitude

Figure 8. Influence of different factors on the shimmy region

Table. 3. Influence of braking frequency and amplitude on shimmy region

frequency	stable area	torsional dominant area	lateral dominant area	amplitude	stable area	torsional dominant area	lateral dominant area
10Hz	501	393	1606	9000	501	393	1606
5Hz	+2.9%	+22.9%	-6.5%	7000	-6.8%	-14.5%	+5.7%
15Hz	-7.4%	-18.8%	+6.9%	11000	+2.9%	+15.5%	-3.1%

3.4. *Influence of Braking Frequency on Oscillation Amplitude*

Take a point D(V=30m/s,F_z=161KN) in figure 8 (a) and analyze the influence of braking frequency change on the oscillation characteristics of the point on the region boundary. The results are shown in figure 9. It can be seen from figure 9 that the influence of braking frequency on the oscillation characteristics at this point is mainly reflected in the torsional shimmy. With the increase of braking frequency, the amplitude of torsional shimmy is suppressed. When the braking frequency increases from 5Hz to 10Hz, the torsional shimmy motion of the system contains multiple frequency components. When the braking frequency further increases to 15Hz, the frequency of torsional shimmy of the system gradually tends to be stable. According to the above analysis, when the load value of the landing gear strut is located near the boundary of the torsional region in figure 8, appropriately increasing the braking frequency can effectively reduce the amplitude of the torsional shimmy and reduce the impact of the shimmy on the landing gear structure.

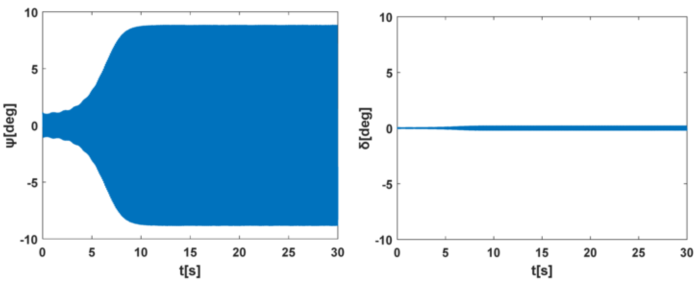

(a) f=5Hz

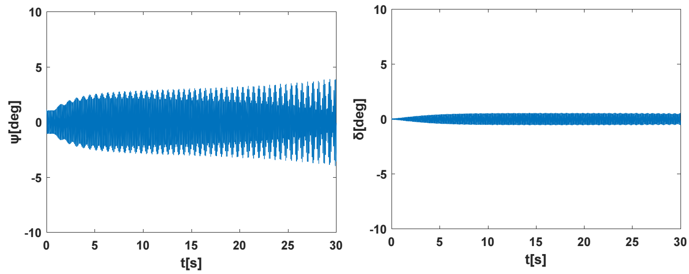

(b) f=10Hz

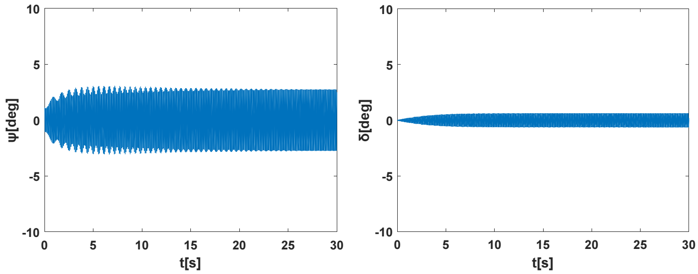

(c) f=15Hz

Figure 9. Influence of braking frequency on oscillation amplitude

4. Conclusion

In this paper, a mathematical model describing the nose gear shimmy under braking condition is established, and the influence of anti-skid braking system on the nose gear shimmy is studied. The main conclusions are as follows:The implementation of anti-skid braking system will reduce the area of torsional shimmy region and stable region in the whole parameter space, and increase the area of lateral shimmy region. Increasing the braking frequency will further reduce the area of the torsional and stable regions, and increase the area of the lateral region. The effect of increasing the braking amplitude on the shimmy region is opposite to that of increasing the braking frequency. Increasing the braking frequency can effectively suppress the increase of torsional shimmy, but the effect on restraining the amplitude of lateral shimmy is limited.

Acknowledgment

The author would like to thank Youth Project of Humanities and Social Sciences of the Ministry of Education of China(Grant No.20YJC880087), Management Science Open Competition Project supported by the Science and Technology Department of Jiangxi Province(Grant No. 20212BAA10011), Special Foundation Project for Postgraduate Innovation of Nanchang Hangkong University(Grant No.YC2021-028) for the funding support to this study.

References

[1] Rahmani M, Behdinan K. Investigation on the effect of coulomb friction on nose landing gear shimmy[J]. *Journal of Vibration and Control*, 2019, 25(2): 255-272.

[2] Von Schlippe B, Dietrich R. Shimmying of a pneumatic wheel[R]. Washington D.C.:NACA,1947.

[3] Thota P, Krauskopf B, Lowenberg M. Interaction of torsion and lateral bending in aircraft nose landing gear shimmy[J]. *Nonlinear dynamics*, 2009, 57(3): 455-467.

[4] Thota P, Krauskopf B, Lowenberg M. Bifurcation analysis of nose-landing-gear shimmy with lateral and longitudinal bending[J]. *Journal of Aircraft*, 2010, 47(1): 87-95.

[5] Thota P, Krauskopf B, Lowenberg M. Multi-parameter bifurcation study of shimmy oscillations in a dual-wheel aircraft nose landing gear[J]. *Nonlinear dynamics*, 2012, 70(2): 1675-1688.

[6] Arreaza C, Behdinan K, Zu J. Linear stability analysis and dynamic response of shimmy dampers for main landing gears[J]. *Journal of Applied of Mechanics*, 2016, 83(8):081002.

[7] Rahmani M, Behdinan K. On the effectiveness of shimmy dampers in stabilizing nose landing gears[J]. *Aerospace Science and Technology*, 2019, 91: 272-286.

[8]Rahmani M, Behdinan K. Interaction of torque link freeplay and Coulomb friction nonlinearities in nose landing gear shimmy scenarios[J]. *International Journal of Non-Linear Mechanics*, 2020, 119: 103338.

[9]Thota P, Krauskopf B, Lowenberg M, et al. Influence of tire inflation pressure on nose landing gear shimmy[J]. *Journal of Aircraft*, 2010, 47(5): 1697-1706.

[10]Feng F, Lou B, Zhang C, et al.Effect of wheel-distance and corotating wheels on aircraft shimmy[J]. *Journal of Vibration and Shock*,2019,38(06):212-217.

[11]Feng F, Nie H, Zhang M, et al. Effect of torsional damping on aircraft nose landing-gear shimmy[J]. *Journal of Aircraft*, 2015, 52(2): 561-568.

[12]Yin Q Z, Nie H, Zhang M, et al. Vibration characteristics of gear walk on half-axle landing gear [J]. *Journal of Vibration Engineering*,2016,29(06):954-962.

[13]Yin Q Z. Research on the stability of UAV low frequency braking and ground taxiing [D]. Nanjing University of Aeronautics and Astronautics,2018.

[14]Chen S, Yin Q Z, Song J Y, et al. Research on low frequency coupled brake-induced vibration of telescopic landing gear with two wheels[J/OL]. *Advances in Aeronautical Science and Engineering*: http://kns.cnki.net/kcms/detail/61. 1479.V.20220130.1024.002. html [2022-03-11].

[15] Ran S, Besselink I, Nijmeijer H. Application of nonlinear tyre models to analyse shimmy[J]. *Vehicle System Dynamics*, 2014, 52(1): 387-404.

[16]Wu S, Pang B, Wei R L, et al.A hardware-in-the-loop simulation system for aircraft braking[J]. *Transactions of Beijing Institute of Technology*,2020,40(02):189-192+197.

[17]Pecora R. A Rational Numerical Method for Simulation of Drop-Impact Dynamics of Oleo-Pneumatic Landing Gear[J]. *Applied Sciences*, 2021, 11(9): 4136.

[18]Garza P, Perinpanayagam S, Aslam S, et al. Qualitative Validation Approach Using Digital Model for the Health Management of Electromechanical Actuators[J]. *Applied Sciences*, 2020, 10(21): 7809.